AIAA 81-4347

# Design and Off-Design Performance Calculations of Space Radiators

Masao Furukawa*
*National Space Development Agency of Japan, Tokyo, Japan*

**An analysis has been carried out to develop simplified algorithms which are helpful in the design problem of space radiators and in performance calculations for off-design operating conditions. Five types of space radiators with liquid coolant circulation are taken into consideration. They are a plane radiator without heat pipes (type 1), one with conventional heat pipes (type 2), one with variable conductance heat pipes (type 3), a conical radiator associated with a nuclear reactor (type 4), and a tube with radiative fins forming V-cavities (type 5). The variational method is employed to obtain an analytical solution of a nonlinear differential equation which governs the heat balance of a radiator panel exposed to solar radiation. This solution permits the calculation of inlet and outlet liquid temperatures, which must be within allowable limits specified by design requirements. One then applies the flat-front theory to the estimation of active lengths of variable conductance heat pipes. This paper presents several figures for design practice of radiators of type 3. They can be used to determine the optimal reservoir volume and the reservoir temperature which should be controlled in response to the heat rejection rate. The optimal quantity of control gas depends on the nature of working fluids. The fluids investigated are ammonia, Freon-11, Freon-21, and methyl alcohol. Parametric studies are then made to optimize the dimensions of a type 4 radiator and to analyze the effect of fin surface nondiffusiveness on the performance of a type 5 radiator.**

## Nomenclature

$A$ = cross-sectional area
$a$ = coefficient specified as Eqs. (52), relating to Eq. (51)
$B$ = absorption factor, given in Eq. (A10) or (A11)
$b,b'$ = coefficients defined in Eq. (5) or (59)
$C_p$ = specific heat of liquid at constant pressure
$c$ = coefficient defined in Eqs. (18), (36), (42), or (65)
$H_s$ = factor specifying solar direction, defined in Eq. (62) or (A14)
$h$ = fin thickness
$h_f$ = heat transfer coefficient between liquid and tube
$I_s$ = solar constant
$J$ = functional defined in Eqs. (16), (34), or (40)
$L$ = length
$m$ = mass of radiator panel or cone
$N$ = number of tubes or heat pipes
$N_g$ = number of moles of control gas
$p$ = vapor pressure, given in Eq. (51)
$p_s$ = vapor pressure at $T_s$
$p_w$ = wetted perimeter of tube
$Q$ = heat load
$q$ = heat absorbed per unit fin surface, given in Eqs. (9), (61), or (A12)
$R$ = universal gas constant
$r$ = radius of cylinder or cone
$T$ = absolute temperature
$T_s$ = equivalent sink temperature, defined in Eq. (9)
$u$ = emissive power, defined in Eq. (69)
$V$ = volume
$W$ = half-interval between tubes or heat pipes
$X,Z$ = length coordinates
$x,z$ = dimensionless coordinates, defined in Eq. (11) or in Eq. (3) or (20)
$\alpha$ = solar absorptance
$\beta$ = coefficient defined in the first expression of Eq. (14) or (64)
$\gamma$ = coefficient defined in the second expression of Eq. (14) or (64)
$\delta$ = half-cone angle, shown in Fig. 2
$\epsilon$ = infrared emittance
$\theta$ = dimensionless temperature, defined in Eqs. (12), (31), or (38)
$\theta_s$ = solar elevation angle, shown in Fig. 2 or 3
$\lambda$ = heat conductivity of fin material
$\bar{\lambda}$ = effective conductance per unit length
$\mu$ = liquid-temperature ratio, defined in Eq. (2)
$\rho$ = reflectance
$\sigma$ = Stefan-Boltzmann constant
$\phi$ = angle defined in Eq. (56), shown in Fig. 3
$\varphi_s$ = solar azimuth angle, shown in Fig. 2 or 3
$\dot{\omega}_f$ = liquid flow rate

*Subscripts*

$a$ = active condenser section
$B$ = fin root
$c$ = condenser section
$D$ = diffuse component
$e$ = evaporator section
$f$ = liquid coolant
$n$ = number to identify fin, tube, heat pipe, or cavity
$R$ = reservoir
$S$ = specular component
$V$ = vapor
in = inlet
out = outlet

*Superscript*

$(\ )^*$ = solar wavelength region

Received Aug. 27, 1980; revision received July 22, 1981. 

*Engineer, First Group of Satellite Design.

## Introduction

THE use of space radiators has recently become of great importance to thermal design and control as spacecraft become voluminous, complex, and high in electrical power consumption. Pumped liquid radiators with flat fin panels are convectional types of radiators put into space use. For such a radiator, Russell and Chapman[1,2] presented an analytical solution for transient temperature distribution in a one-dimensional radiating fin and computational procedure for performance of a radiator system operating at off-design conditions. Their results being of special interest are the

analytical representations of liquid temperatures in the known-heat-load case where the heat rejection rate and the tube length are given. Such a case frequently occurs for a radiator system designed for a maximum heat load but operating with a lower load. However, their analyses are based on zero irradiation environment and, in addition, the results seem rather complicated for design purposes.

Roukis, Rogovin, and Swerdling[3] first made feasibility studies on heat pipe applications to space radiators. They demonstrated that heat pipe radiator systems are lighter than conventional fluid loop coolant systems. Since a puncture occurring in a heat pipe gives rise to only a minimum change in radiator performance, a particular benefit of heat pipe radiators is reduced meteoroid vulnerability. Their idea was later developed by Edelstein[4] who designed and tested several types of heat pipe radiators having deployment capability. Based on the numerical and experimental results, he found a type which met the design goals. Ward[5] then conducted thermal vacuum tests to measure the performance of a variable conductance heat pipe radiator of the type selected by Edelstein.[4] For reducing costs and augmenting application flexibility, Alario and his co-workers[6,7] developed a heat pipe radiator panel of modular construction, helping to enhance shuttle mission capabilities. Then Schlitt[8] applied a heat pipe radiator to high-power shunt electronics for thermal control of communications satellites and conducted a parametric study to select an optimal layout of the radiator.

Although the radiators mentioned above are plane-shaped, there are two other kinds of space radiator configurations. The first is closely related with a powerplant which utilizes a liquid-metal-cooled nuclear reactor. In this connection, Tharpe and Arker[9] designed the SNAP-8 power conversion system composed of an electromagnetic pump and a radiator cone. Keil[10] then developed a computer program to optimize mass and structure of a conical radiator connected with a neutron shield. The second is a radiator consisting of a tube with radiatively interacting V-groove fins. Hering[11] analyzed the radiative transfer in such a groove and presented an analytical expression of the solar radiosity function. Schnurr[12] then computed the heat transfer rate from an array of fins of triangular profile. Further advances are still necessary in analytical studies because of few expressions[3-12] suitable for engineering calculations.

The primary purpose of this paper is to present an algorithm which can be readily applied to development of software utilizable for design optimization and performance evaluation of a radiator system. A systematic attempt is made to permit treatment of various types of space radiators. Some comparisons with test results[4,5] are presented to verify the solution method. The results of parametric studies are summarized in tables and figures, some of which will serve to establish design and operation guidelines for heat pipe radiators recognized as an attractive means of spacecraft temperature control.

## Analysis

### Fin-and-Tube Plane Radiator (type 1)

The upper part of Fig. 1 shows a schematic of a conventional pumped-liquid radiator consisting of $N$ tubes and $N+1$ fins. The tubes are placed at regular intervals of $2W$ on a rectangular fin panel of the length $L$ and $2NW$ in width. In this system, the heat, dissipated in onboard equipment and transferred by cooling liquid circulation, is finally released from radiating fins to space. The liquid temperature thereby decreases from $T_{in}$ in the inlet to $T_{out}$ in the outlet. From a viewpoint of operation in orbit, the radiator needs to be so designed as to keep the outlet temperature nearly constant over a range of heat load variation. For this reason, an analysis should be first attempted for the coolant liquid flow. The following assumptions are made in the analysis: 1) negligible conduction in the fluid; 2) negligible viscous dissipation in the fluid; 3) constant fluid properties; and 4) low flow rates.

Based on the theorem of minimum entropy production or on an infinitesimal energy balance on the fluid, Russell and Chapman[1] found the following expression giving a liquid temperature profile along the tube length:

$$T_f = T_{in}\mu^z \tag{1}$$

where $\mu$ and $z$ are defined as:

$$\mu = T_{out}/T_{in} \tag{2}$$

$$z = Z/L \tag{3}$$

The coordinate system is shown in Fig. 1, but the dimensionless coordinate defined in Eq. (3) is used for convenience. In deriving Eq. (1), Russell and Chapman[1] made the following assumption:

$$T_B = bT_f \tag{4}$$

Equation (4) is a simplified expression between the liquid bulk and tube wall temperatures, and according to their estimation this expression is valid to such a degree that the error remains less than 1% for representative radiator systems. The coefficient $b$ is here expressed as:

$$b = 1 + (C_p\dot{\omega}_f/h_f p_w L)\log\mu \tag{5}$$

Equation (5) is obtained by substituting Eqs. (1) and (4) into a differential equation which governs the convective heat transfer from the liquid to the wall. A basic relationship for the heat loss of the coolant liquid is:

$$Q = C_p\dot{\omega}_f(T_{in} - T_{out}) = C_p\dot{\omega}_f T_{in}(1-\mu) \tag{6}$$

This expression serves as a common basis of radiator performance calculations.

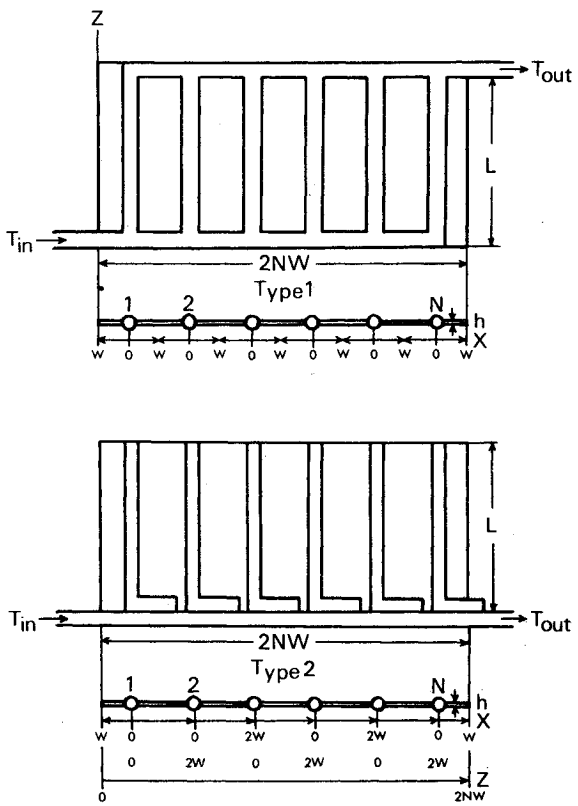


Fig. 1 Geometry of plane radiators (types 1 and 2).

In order to solve the unknown temperatures $T_{in}$ and $T_{out}$ for the known heat load $Q$, two independent relations are necessary. One of them is Eq. (6), while the other can be derived from an expression describing the conductive heat flux at the fin root ($X=0$). For the fin analysis, the assumption is made that the fin conducts heat only in a direction perpendicular to the tube, that is, in the positive $X$ direction. For engineering purposes, the error due to this simplification is acceptable because the numerical results differ less than 1% from those of detailed nodal network analyses[1] which account for both lateral and longitudinal conduction in the fin. Since this assumption renders the problem one-dimensional, the conductive heat transfer is estimated at $-2\lambda h(dT/dX)_{X=0}dZ$ for an elemental longitudinal distance $dZ$. The total heat transfer is obtained by integrating this expression over all the tube length. The result becomes $Q/N$ because the heat load is distributed to each tube in an equal manner resulting in the following expression:

$$Q=-2N\lambda h\int_0^L\left(\frac{dT}{dX}\right)_{X=0}dZ \tag{7}$$

The problem is now to reduce Eq. (7) to a more convenient form. Attention is therefore turned to finding a steady-state fin temperature distribution from which the temperature gradient can be calculated at the fin root. As seen from Fig. 1, every fin originates from a tube ($X=0$) and extends as far as a midpoint ($X=W$) or an edge ($X=W$) of the panel. In addition to this geometrical identity, there is no difference between any two fins in thermal properties. Thus one has only to consider a fin extending over the range $0\leq X\leq W$. In this region, the thermal balance of an infinitesimal fin element $dX$ on a double-sided radiator is governed by the following nonlinear differential equation:

$$\lambda h\frac{d^2T}{dX^2}=(\epsilon_0+\epsilon)\sigma T^4-q_0 \tag{8}$$

where $q_0$ is expressed as:

$$q_0=\epsilon_0\sigma T_s^4 \tag{9}$$

Equation (9) shows the incoming radiation absorbed in the outside fin surface of the emittance $\epsilon_0$, where the irradiation environment is specified by the equivalent sink temperature $T_s$. The boundary conditions to be considered are:

$$T(0)=T_B \qquad T'(W)=0 \tag{10}$$

For a nondimensional approach, one introduces the following new variables:

$$x=X/W \tag{11}$$

$$\theta=T/T_B \tag{12}$$

By using Eqs. (11) and (12), Eq. (8) is rewritten as:

$$\frac{d^2\theta}{dx^2}=\gamma T_B^3\theta^4-\frac{\beta}{T_B} \tag{13}$$

where $\beta$ and $\gamma$ are defined as:

$$\beta=\frac{q_0W^2}{\lambda h} \qquad \gamma=\frac{(\epsilon_0+\epsilon)\sigma W^2}{\lambda h} \tag{14}$$

Equation (10) then becomes:

$$\theta(0)=1 \qquad \theta'(1)=0 \tag{15}$$

The difficulty in solving Eq. (13) is nonlinearity such as $\theta^4$, but the variational method provides an analytical means which can deal with this difficulty. Application of the variational principle to the boundary value problem defined in Eqs. (13) and (15) leads to the following functional:

$$J=\int_0^1\left\{\left(\frac{d\theta}{dx}\right)^2+\frac{2}{5}\gamma T_B^3\theta^5-\frac{2\beta}{T_B}\theta\right\}dx \tag{16}$$

It is easily proved that an extremum of Eq. (16) is equivalent to the solution of Eq. (13). An approximate expression of the extremum can be found by the use of the Ritz procedure. The following expression satisfying Eq. (15) is a test function employed with a view to minimizing Eq. (16):

$$\theta=1-c(2x-x^2) \tag{17}$$

The optimal value of the unknown coefficient $c$ is determined in such a way that $dJ/dc=0$ where $J$ is a reduced expression obtained by substituting Eq. (17) into Eq. (16):

$$c=\frac{23}{40}\left(\gamma T_B^3-\frac{\beta}{T_B}\right)\left(1+\frac{8}{5}\gamma T_B^3\right)^{-1} \tag{18}$$

Equation (7) is now expressed as follows by using Eqs. (3), (11), (12), and (17):

$$Q=\frac{4N\lambda hL}{W}\int_0^1 cT_Bdz \tag{19}$$

Equation (19) associated with Eqs. (1), (4), and (18) can be numerically computed, and the result permits the estimation of the outlet-to-inlet temperature ratio. Thus the inlet liquid temperature is derived from Eq. (6).

**Fixed Conductance Heat Pipe Radiator (type 2)**

The radiator shown in the lower part of Fig. 1 is the least complicated type of heat pipe radiator, which consists of L-shaped, fixed conductance heat pipes directly coupled to the fluid header. Each of the heat pipes is $L_e$ in evaporator length, $L_c$ in condenser length, and the same in thermal characteristics. The geometry is identical to a radiator of type 1, expect that the fluid tubes are replaced with heat pipes, but the coordinate system is different from that for type 1. The $Z$ axis runs parallel to the fluid header in a direction of liquid flow. The $X$ axes are also parallel to the fluid header. The radiator panel is composed of $N+1$ fins: the $n$th fin ($n=1,2,\ldots,N-1$) forms a rectangular plane between the $n$th ($X=0$) and $n+1$th ($X=2W$) heat pipes; but the zeroth or $N$th fins, originated from the first or $N$th heat pipes, extend as far as the left or right edges ($X=W$) of the panel, respectively.

As distinct from the radiator of type 1, the passage distance of coolant liquid is not $L$ but $2NW$. The following new coordinate is therefore employed in place of Eq. (3):

$$z=Z/2NW \tag{20}$$

Because of the similarity law on liquid temperature distributions, Eq. (1) holds good as before. A basic quantity derived from Eq. (1) is the heat transmitted to the $n$th heat pipe. This heat supply, denoted as $Q_n$, is equal to the energy loss in the liquid streaming down the interval $(n-1)/N\leq z\leq n/N$; and, hence, is given by the following expression:

$$Q_n=C_p\dot{\omega}_fT_{in}(\mu^{(n-1)/N}-\mu^{n/N}) \tag{21}$$

Taking the average of Eq. (1) over the above interval, one has the mean liquid temperature:

$$T_{fn}=-NQ_n/C_p\dot{\omega}_f\log\mu \tag{22}$$

Equation (22) gives plots ($z=1/2N,\ 3/2N,\ldots,(2N-1)/2N$) of a liquid temperature distribution ($0\le z\le 1$).

The heat, specified as $Q_n$, is conducted from the header wall to the evaporator section, and then transferred to the condenser section with a vapor flow of the working fluid in the heat pipe. This heat transfer can be simply formulated as:

$$Q_n=\bar{\lambda}_e L_e(T_{fn}-T_{Vn}) \tag{23}$$

$$Q_n=\bar{\lambda}_c L_c(T_{Vn}-T_{Bn}) \tag{24}$$

where $\bar{\lambda}_e$ and $\bar{\lambda}_c$ are the effective heat conductance per unit length of the liquid-to-vapor interface and that of the vapor-to-fin interface, respectively. The vapor temperature drop in the condenser section is not taken into account because this effect is generally very small. The vapor temperature in the $n$th heat pipe and the fin root temperature of the $n$th fin, $T_{Vn}$ and $T_{Bn}$, are readily derived from Eqs. (22), (23), and (24):

$$T_{Vn}=Q_n(-N/C_p\dot{\omega}_f\log\mu-1/\bar{\lambda}_e L_e) \tag{25}$$

$$T_{Bn}=Q_n\{-N/C_p\dot{\omega}_f\log\mu-(1/\bar{\lambda}_e L_e+1/\bar{\lambda}_c L_c)\} \tag{26}$$

In setting up Eqs. (23) and (24), it is assumed that the heat is uniformly dissipated in the condenser section, and that there is no heat soak from the evaporator section to the fin panel.

Because of the above assumptions, the problem becomes one-dimensional. Hence the temperature gradient along the $X$ axis is constant at any point of the fin root. This results in the following expressions which are basically equivalent to Eq. (7):

$$Q_1=\lambda h L_c\left\{-\left(\frac{dT_0}{dX}\right)_{X=0}-\left(\frac{dT_1}{dX}\right)_{X=0}\right\} \tag{27a}$$

$$Q_n=\lambda h L_c\left\{\left(\frac{dT_{n-1}}{dX}\right)_{X=2W}-\left(\frac{dT_n}{dX}\right)_{X=0}\right\} \qquad (n=2,3,\ldots,N) \tag{27b}$$

where $T_n(X)$ represents a temperature distribution of the $n$th fin. Equations (27) show that the heat transmitted through the $n$th heat pipe is conducted to the $n-1$th and $n$th fins in accordance with Fourier's law. Adding up all the expressions given by Eqs. (27), one has the total heat transfer which will be equal to the heat load specified as Eq. (6):

$$Q=\sum_{n=1}^{N} Q_n \tag{28}$$

The subsequent analysis is made to determine a steady-state fin temperature distribution. As regards the $n$th fin ($n=1,2,\ldots,N-1$), steady states are governed by the same expression as Eq. (8):

$$\lambda h\frac{d^2T_n}{dX^2}=(\epsilon_0+\epsilon)\sigma T_n^4-q_0 \tag{29}$$

But the boundary conditions associated with Eq. (29) are different from Eq. (10):

$$T_n(0)=T_{Bn} \qquad T_n(2W)=T_{Bn+1} \tag{30}$$

Equation (12) is expressed as:

$$\theta_n=T_n/T_{Bn} \tag{31}$$

By using Eqs. (11) and (31), Eq. (29) is rewritten as:

$$\frac{d^2\theta_n}{dx^2}=\gamma T_{Bn}^3\theta_n^4-\frac{\beta}{T_{Bn}} \tag{32}$$

Equation (30) then becomes:

$$\theta_n(0)=1 \qquad \theta_n(2)=T_{Bn+1}/T_{Bn} \tag{33}$$

The variational method can be also employed to solve the boundary value problem defined in Eqs. (32) and (33). According to this method, the problem is attributed to finding an extremum of the following functional:

$$J_n=\int_0^2\left\{\left(\frac{d\theta_n}{dx}\right)^2+\frac{2}{5}\gamma T_{Bn}^3\theta_n^5-\frac{2\beta}{T_{Bn}}\theta_n\right\}dx \tag{34}$$

Easily proved, the extremum gives a solution of Eq. (32). For minimizing Eq. (34), one employs the Ritz procedure. This requires a test function to be introduced. The following expression satisfying Eq. (33) is taken here as the test function:

$$\theta_n=1+(T_{Bn+1}/T_{Bn}-1)x/2-c_n(2x-x^2) \tag{35}$$

The integrations in Eq. (34) are carried out by using Eq. (35) to reduce the expression of $J_n$. The unknown coefficient $c_n$ ($n=1,2,\ldots,N-1$) is derived from the relation $dJ_n/dc_n=0$:

$$c_n=\frac{23}{40}\left\{\gamma T_{Bn}^2(2T_{Bn+1}-T_{Bn})-\frac{\beta}{T_{Bn}}\right\}\times\left\{1+\frac{4}{5}\gamma T_{Bn}^2(3T_{Bn+1}-T_{Bn})\right\}^{-1} \tag{36}$$

Now one considers the zeroth and $N$th fins. The temperature distributions are also governed by Eq. (32) because all fins are the same in thermal properties. The boundary conditions are, however, different from Eq. (30):

$$T_0(0)=T_{B1},\quad T_0'(W)=0;\quad T_N(0)=T_{BN},\quad T_N'(W)=0 \tag{37}$$

The second and fourth expressions of Eq. (37) show that there is no conductive heat loss from both edges of the panel. The following expression is then substituted for Eq. (31):

$$\theta_0=T_0/T_{B1} \qquad \theta_N=T_N/T_{BN} \tag{38}$$

By using Eqs. (11) and (38), Eq. (37) is rewritten as:

$$\theta_n(0)=1 \qquad \theta_n'(1)=0 \qquad (n=0,N) \tag{39}$$

Because of Eq. (39), the functional resulted from Eq. (32) is different from Eq. (34) in the upper limit of the integral:

$$J_n=\int_0^1\left\{\left(\frac{d\theta_n}{dx}\right)^2+\frac{2}{5}\gamma T_{Bn}^3\theta_n^5-\frac{2\beta}{T_{Bn}}\theta_n\right\}dx \tag{40}$$

Since Eq. (39) is essentially the same as Eq. (15), the same expression as Eq. (17) is employed as a test function to minimize Eq. (40):

$$\theta_n=1-c_n(2x-x^2) \tag{41}$$

Substitution of Eq. (41) into Eq. (40) leads to a reduced expression of $J_n$. The unknown coefficient $c_n$ ($n=0,N$) is determined so that $dJ_n/dc_n=0$:

$$c_0=\frac{23}{40}\left(\gamma T_{B1}^3-\frac{\beta}{T_{B1}}\right)\left(1+\frac{8}{5}\gamma T_{B1}^3\right)^{-1} \tag{42a}$$

$$c_N=\frac{23}{40}\left(\gamma T_{BN}^3-\frac{\beta}{T_{BN}}\right)\left(1+\frac{8}{5}\gamma T_{BN}^3\right)^{-1} \tag{42b}$$

The temperature gradients at the fin roots can now be estimated by using Eqs. (35) and (41). Equations (27) are thereby reduced to the expressions which yield the following result:

$$Q=\frac{2\lambda hL_c}{W}\left(c_0T_{B1}+2\sum_{n=1}^{N-1}c_nT_{Bn}+c_NT_{BN}\right) \tag{43}$$

where $c_0$, $c_N$, and $c_n$ are given by Eqs. (42) and (36). The known-heat-load problem becomes then solvable by the use of Eqs. (43) and (6).

**Variable Conductance Heat Pipe Radiator (type 3)**

The performance of heat pipe radiators may be improved by building variable conductance into the feeder heat pipes. This new type is similar to type 2 except that a gas reservoir is added to the condenser end. The configuration and the coordinate system are the same as those shown in the lower part of Fig. 1. The analytical results, obtained in the previous section, are therefore applicable to this system. However, Eq. (24) needs to be modified because there exists a gas-blocked region being inactive as the condenser. This fact can be expressed in terms of the active condenser length. Thus Eq. (24) is rewritten as:

$$Q_n=\bar{\lambda}_cL_{an}(T_{Vn}-T_{Bn}) \tag{44}$$

Because of this expression, Eq. (26) becomes:

$$T_{Bn}=Q_n\{-N/C_p\dot{\omega}_f\log\mu-(1/\bar{\lambda}_eL_e+1/\bar{\lambda}_cL_{an})\} \tag{45}$$

where $Q_n$ is given by Eq. (21).

In response to the above change, Eqs. (27) turn into the following expressions:

$$Q_1=\lambda hL_{a1}\left\{-\left(\frac{dT_0}{dX}\right)_{X=0}-\left(\frac{dT_1}{dX}\right)_{X=0}\right\} \tag{46a}$$

$$Q_n=\lambda hL_{an}\left\{\left(\frac{dT_{n-1}}{dX}\right)_{X=2W}-\left(\frac{dT_n}{dX}\right)_{X=0}\right\} \quad (n=2,3,\ldots,N) \tag{46b}$$

The differential derivatives in Eqs. (46) are evaluated by using Eqs. (31), (35), (38), and (41). Equation (28) is thereby expressed as:

$$\begin{aligned}Q=\frac{\lambda h}{W}\Big[&L_{a1}\{2T_{B1}(c_0+c_1)+(T_{B1}-T_{B2})/2\}\\&+\sum_{n=2}^{N-1}L_{an}\{2(T_{Bn-1}c_{n-1}+T_{Bn}c_n)+(2T_{Bn}-T_{Bn-1}\\&-T_{Bn+1})/2\}+L_{aN}\{2(T_{BN-1}c_{N-1}+T_{BN}c_N)\\&+(T_{BN}-T_{BN-1})/2\}\Big]\end{aligned} \tag{47}$$

where $c_n$ $(n=0,1,\ldots,N)$ and $T_{Bn}$ $(n=1,2,\ldots,N)$ are given by Eq. (36) or (42) and by Eq. (45), respectively. If $L_{an}=L_c$ for all the heat pipes, Eq. (47) then reduces to Eq. (43). Such a case occurs when the heat is supplied over a specified limit.

The fin root temperature is predictable from Eq. (45) provided that the active condenser length can be estimated. The flat-front theory[13,14] provides a simple mathematical model describing the formation of a gas plug in the condenser section which acts as a diffusion barrier to the vapor flow. The model is based on the following assumptions: 1) the interface between the active and shut-off portions is very sharp; 2) the total pressure is uniform throughout the heat pipe; 3) the vapor-gas mixture is ideal; and 4) the molar noncondensible gas inventory remains constant for all operating conditions. The gas temperature is $T_s$ in the inactive portion of the condenser and $T_R$ in the hot nonwicked reservoir. The partial pressure of the control gas is then equal to $p_n-p_s$ in both regions where $p_n$ and $p_s$ are the vapor pressure at $T_{Vn}$, given by Eq. (25), and that at $T_s$, respectively. In each region, the molar gas inventory is determined from the equation of state of perfect gas. This results in the following expression:

$$N_g=\frac{(p_n-p_s)A_V(L_c-L_{an})}{RT_s}+\frac{(p_n-p_s)V_R}{RT_R} \tag{48}$$

where $L_c-L_{an}$ shows the inactive condenser length. Equation (48) is then transformed into:

$$\frac{L_{an}}{L_c}=1+\frac{V_RT_s}{V_cT_R}-\frac{N_gRT_s}{V_c(p_n-p_s)} \tag{49}$$

with the relation:

$$V_c=A_VL_c \tag{50}$$

An estimate of the active condenser length can be thus made if $p_n$ is known. For fluids of interest, vapor pressure data are readily taken from the literature[15-17] but, for convenience, one employs an empirical formula of fairly good accuracy:

$$p=\exp(a_0-a_1/T_V-a_2/T_V^2) \tag{51}$$

where $p$ is expressed in N/m and $T_V$ in K. Typical values of the coefficients $a_0$, $a_1$, and $a_2$ are as follows:

$a_0=2.1969\times10$, $a_1=2.1228\times10^3$, $a_2=9.1527\times10^4$

for $NH_3$ (52a)

$a_0=2.0870\times10$, $a_1=2.4047\times10^3$, $a_2=1.1012\times10^5$

for Freon-11 (52b)

$a_0=2.1888\times10$, $a_1=2.8417\times10^3$, $a_2=1.6991\times10^4$

for Freon-21 (52c)

$a_0=2.3365\times10$, $a_1=3.5206\times10^3$, $a_2=1.6385\times10^5$

for $CH_3OH$ (52d)

Now one considers another type[4,5] of variable conductance heat pipe radiator, type 3′, replacing a fluid line header with a fixed conductance heat pipe to which load is provided from a heat exchanger. Since the condensation rate of a vapor flow is almost uniform in the header condenser section, the load is equally distributed over all the feeder heat pipes. Hence every pipe works in an identical fashion that $T_{Bn}=T_B$, $T_{Vn}=T_V$, $p_n=p$, and $L_{an}=L_a$ $(n=1,2,\ldots,N)$. Equations (28) and (44) and Eq. (47) are thereby reduced to the following expressions:

$$T_V=T_B(1+4\lambda hc/\bar{\lambda}_cW) \tag{53}$$

$$Q=4N\lambda hL_aT_Bc/W \tag{54}$$

where $c$ is written as Eq. (18). The three unknowns $T_B$, $T_V$, and $L_a$ can be numerically determined from Eqs. (53), (54), and (49).

**Fin-and-Tube Conical Radiator (type 4)**

Figure 2 shows a fin-and-tube conical radiator of which the upper and lower radii and the length are $r_1$, $r_2$, and $L$, respectively. The radiator consists of $N$ tubes and $N$ fins. Every fin is trapezoidal as seen from Fig. 2, and the $n$th fin is bordered by the $n$th and $n+1$th tubes. One end of the $n$th tube

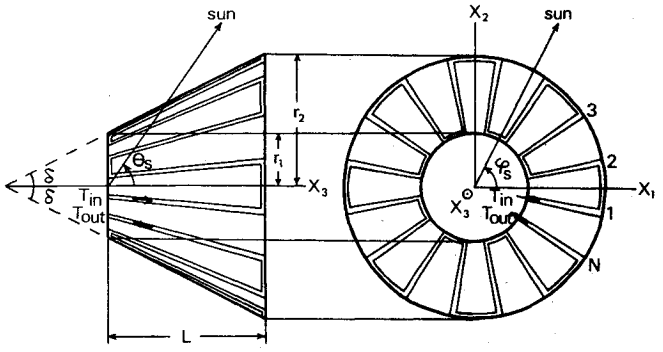


**Fig. 2 Conical radiator (type 4) and solar direction.**

is connected with that of the $n+1$th tube, and thereby the liquid passage distance becomes $NL/\cos\delta$ where $\delta$ is the half-apex angle of the radiator cone.

Because of such a geometry, one meets with a difficulty in the analysis of radiators of this type. But the difficulty can be overcome by a simplification of the geometry. Thus one substitutes a rectangular fin for the trapezoidal fin. The half-fin width is here specified as:

$$W = r\sin\phi \tag{55}$$

This expression is completed with the following relations:

$$\phi = \pi/N \tag{56}$$

$$r = (r_1 + r_2)/2 = r_1 + L\tan\delta/2 \tag{57}$$

Since Eq. (4) is also applicable to this system, the representative temperature of the $n$th tube can be expressed as:

$$T_{Bn} = b' T_{fn} \tag{58}$$

where $T_{fn}$ is given by Eq. (22) but the coefficient $b'$ differs from Eq. (5):

$$b' = 1 + (C_p \dot{\omega}_f \cos\delta / N h_f p_w L)\log\mu \tag{59}$$

The inside surface of the conical radiator is usually thermally insulated; and, hence, the internal radiation exchange can be neglected. The steady-state temperature distributions are, therefore, predictable from the equation slightly different from Eq. (8) or (29):

$$\lambda h \frac{d^2 T_n}{dX^2} = \epsilon\sigma T_n^4 - q_n \tag{60}$$

where $q_n$ is the solar energy absorbed in the $n$th fin:

$$q_n = \alpha I_s H_{sn} \eta(H_{sn}) \tag{61}$$

The function $\eta(H_{sn})$ denotes a Heaviside unit step function which is 1 when $H_{sn} \geq 0$ and 0 when $H_{sn} < 0$. The factor $H_{sn}$ is derived from the inner product between the solar vector and a unit normal vector of the $n$th fin surface:

$$H_{sn} = \sin\theta_s \cos\delta \cos\{\varphi_s - 2\phi(n-1)\} - \cos\theta_s \sin\delta \tag{62}$$

By using Eqs. (11) and (31), Eq. (60) is rewritten as:

$$\frac{d^2\theta_n}{dx^2} = \gamma_0 T_{Bn}^3 \theta_n^4 - \frac{\beta_n}{T_{Bn}} \tag{63}$$

where $\beta_n$ and $\gamma_0$ are defined as:

$$\beta_n = \frac{q_n W^2}{\lambda h} \qquad \gamma_0 = \frac{\epsilon\sigma W^2}{\lambda h} \tag{64}$$

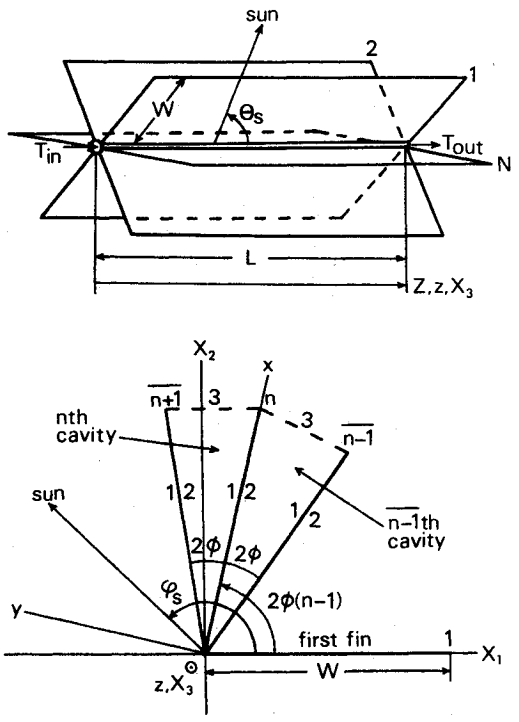


**Fig. 3 Radiatively interacting longitudinal fins (type 5) and solar direction.**

The boundary conditions are also given by Eq. (33), but it should be noted that $T_{B\overline{N+1}}$ is identical to $T_{B1}$. Since Eq. (63) is essentially the same as Eq. (32), the solution is expressed as Eq. (35). The coefficient $c_n$, however, differs from Eq. (36):

$$c_n = \frac{23}{40}\left\{\gamma_0 T_{Bn}^2 (2T_{Bn+1} - T_{Bn}) - \frac{\beta_n}{T_{Bn}}\right\} \times \left\{1 + \frac{4}{5}\gamma_0 T_{Bn}^2 (3T_{Bn+1} - T_{Bn})\right\}^{-1} \qquad (n = 1,\ldots,N-1)$$

$$c_N = \frac{23}{40}\left\{\gamma_0 T_{BN}^2 (2T_{B1} - T_{BN}) - \frac{\beta_N}{T_{BN}}\right\} \tag{65a}$$

$$\times \left\{1 + \frac{4}{5}\gamma_0 T_{BN}^2 (3T_{B1} - T_{BN})\right\}^{-1} \tag{65b}$$

Then one obtains the following expression regarded as a reduced form of Eq. (43):

$$Q = \frac{4\lambda h L}{W} \sum_{n=1}^{N} c_n T_{Bn} \tag{66}$$

**Radiatively Interacting Longitudinal Fins (type 5)**

This is a radiator of technically interesting configuration in which radiant interchange takes place between neighboring fins spaced at regular intervals of the angle $2\phi$. A principal portion of such a radiator is a tube to which are attached $N$ longitudinal fins, $W$ in width and $L$ in length. As seen in Fig. 3, heat is extracted from a liquid that flows through the tube. For analytical treatment of such a configuration, it is sufficient to single out a typical pair of fins as pictured in the lower diagram of the figure. Attention is, therefore, directed to V-groove cavities consisting of the $\overline{n-1}$th, $n$th, $n+1$th fins. In considering net radiation loss from the fins, an energy balance on the $n$th fin yields the following representation:

$$Q_n/WL = 2\epsilon\sigma T_n^4 - 2B_{11}\epsilon\sigma T_n^4 - B_{12}(\epsilon\sigma T_{\overline{n-1}}^4 + \epsilon\sigma T_{\overline{n+1}}^4) - q_n \tag{67}$$

where fin temperatures are assumed to be uniform. Full details of $B_{11}$, $B_{12}$, and $q_n$ are given in the Appendix. In Eq. (67), the second term shows the radiant energy emitted from the $n$th fin and absorbed there again, while the third term expresses the radiation from the $n-1$th or $n+1$th fins which is eventually absorbed in the $n$th fin.

One now employs the following approximation to estimate the heat carried from the liquid to the $n$th fin:

$$Q_n \simeq \frac{3\lambda h L T_B}{4 W u_B}(u_B - u_n) \tag{68}$$

where $u_n$ and $u_B$ are defined as:

$$u_n = \epsilon\sigma T_n^4 \qquad u_B = \epsilon\sigma T_B^4 \tag{69}$$

By using Eqs. (68) and (69), Eq. (67) is rewritten as:

$$2\left(1 - B_{11} + \frac{3\lambda h T_B}{8W^2 u_B}\right)u_n - B_{12}(u_{n-1} + u_{n+1}) = q_n + \frac{3\lambda h T_B}{4W^2} \tag{70}$$

This expression forms simultaneous equations from which the fin temperatures are computed. Taking the average of Eq. (1) over the interval $0 \le z \le 1$, one has the temperature which should be used as $T_B$:

$$T_B = bT_{\text{in}}(\mu - 1)/\log\mu \tag{71}$$

Equations (28) and (68) amount to the heat radiated from all the fins:

$$Q = \frac{3N\lambda h L T_B}{4 W u_B}\left(u_B - \sum_{n=1}^{N} u_n/N\right) \tag{72}$$

The problem is thus attributed to solving Eq. (70). Although Eq. (70) is generally solvable, the solution has a rather sophisticated form. It is, however, simply expressed as follows in the case of no solar heat input ($q_n = 0$):

$$u_n = \frac{3\lambda h T_B}{8W^2}\left(1 - B_{11} - B_{12} + \frac{3\lambda h T_B}{8W^2 u_B}\right)^{-1} \tag{73}$$

Equation (72) then reduces to the following expression:

$$Q = \frac{3N\lambda h L T_B}{4W}(1 - B_{11} - B_{12})\left(1 - B_{11} - B_{12} + \frac{3\lambda h T_B}{8W^2 u_B}\right)^{-1} \tag{74}$$

## Numerical Results and Discussions

First, one deals with a known heat load problem of a type 1 radiator system. The general configuration is representative of the Apollo spacecraft radiator system analyzed by Russell and Chapman.[1] The design parameters are as follows: $L = 3.2$ m, $W = 5.28$ cm, $h = 0.762$ mm, $\lambda = 2.04$ cm·K, $\epsilon_0 = 0.95$, $\epsilon = 0.0$, $C_p = 2.93$ J/g·K, $\dot{\omega}_f = 1.37$ g/s, $h_f = 0.0312$ W/cm²·K, and $p_w = 1.44$ cm. The use of Eqs. (18) and (19) with a load $Q/N$ of 138 W/tube leads to the liquid temperatures that $T_{\text{in}} = 314.3$ K and $T_{\text{out}} = 279.9$ K in case of zero irradiation environment ($T_s = 0$ K). Russell and Chapman[1] present a similar result that $T_{\text{in}} = 313$ K and $T_{\text{out}} = 279$ K. Such a good agreement shows that results based on Eqs. (18) and (19) are so accurate as to require no corrections.

Discussions are continued on type 2, type 3, and type 3′ radiator systems. Each system consists of a fin panel and six feeder heat pipes with ammonia as working fluid. The evaporator length is 30.5 cm; and the panel is 0.813-mm thick, 1.83-m long, and 10.2 cm in half-interval between two consecutive heat pipes. The vapor cross-sectional area is 0.383 cm² in every part of the heat pipe; and, hence, the volume of condenser section amounts to 70.1 cm³. The fins are 2.05 W/cm·K in heat conductivity and 0.90/0.0 in surface properties $\epsilon_0/\epsilon$. The Freon-21 flow rate in a header is 63.0 g/s, and the specific heat of the liquid at constant pressure is 1.05 J/G·K over a specified load range. The header-to-feeder conductance and the feeder-to-fin conductance, $\bar{\lambda}_e$ and $\bar{\lambda}_c$, are 0.666 W/cm·K and 0.924 W/cm·K, respectively, per unit length. Each reservoir is 547 cm³ in volume, and filled with 0.25 mole of gaseous nitrogen. The reservoir temperature is held constant by using thermostatically controlled heaters. All the parameters defined above are the same as those employed by Edelstein[4] who gave plenty of performance test data on heat pipe radiators. This permits direct comparison of analytical predictions with his numerical or experimental results.[4]

For a type 2 radiator system with a load of 200 to 400 W, the results computed from Eqs. (36), (42), and (43) are as follows: $T_{\text{out}} = 248.1$, 260.1, and 274.9 K when $T_s = 194$, 216, and 239 K for the lower load; while, for the upper load, $T_{\text{out}} = 282.0$, 290.7, and 301.8 K at the same sink temperatures. Closely correlated results are given by Edelstein[4]; that is, $T_{\text{out}} = 255$, 262, and 274 K when $Q = 200$ W, while $T_{\text{out}} = 281$, 290, and 301 K when $Q = 400$ W. Correlations between such two predictions in liquid temperatures hold also for a type 3 radiator system. For instance, when $T_s = 216$ K, $T_R = 228$ K, and $Q = 200$ or 400 W, one finds from Eqs. (36), (42), (47), and (49) that $T_{\text{out}} = 292.0$ or 293.6 K. Edelstein[4] then estimates $T_{\text{out}}$ at 291 or 296 K. Thus, the use of Eqs. (36), (42), and (43) or Eqs. (36), (42), (47), and (49) causes no significant errors in solutions of known heat load problems of type 2 or type 3 radiator systems.

Numerical results are now compared with experimental ones. The predicted outlet temperatures of the type 3 radiator system are 291.8, 293.6, and 296.1 K when $T_s = 210$ K, $T_R = 228$ K, and $Q = 240$, 440, and 590 W. The test results[4] corresponding to them are 291, 294, and 298 K, which are marked in Fig. 4. Then, for a type 3′ radiator, the fin root temperatures $T_B$ calculated from Eqs. (53), (54), and (49) are

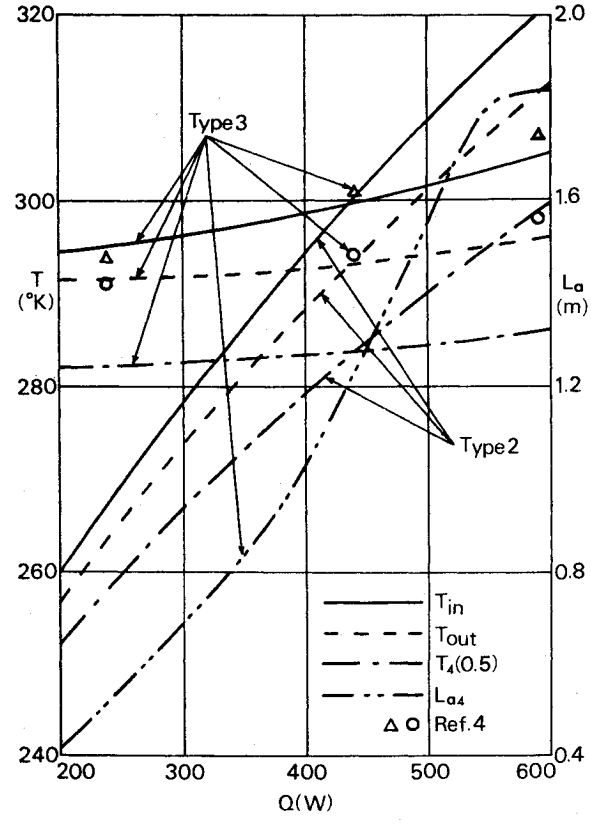


**Fig. 4 Thermal characteristics of heat pipe radiators (types 2 and 3).**

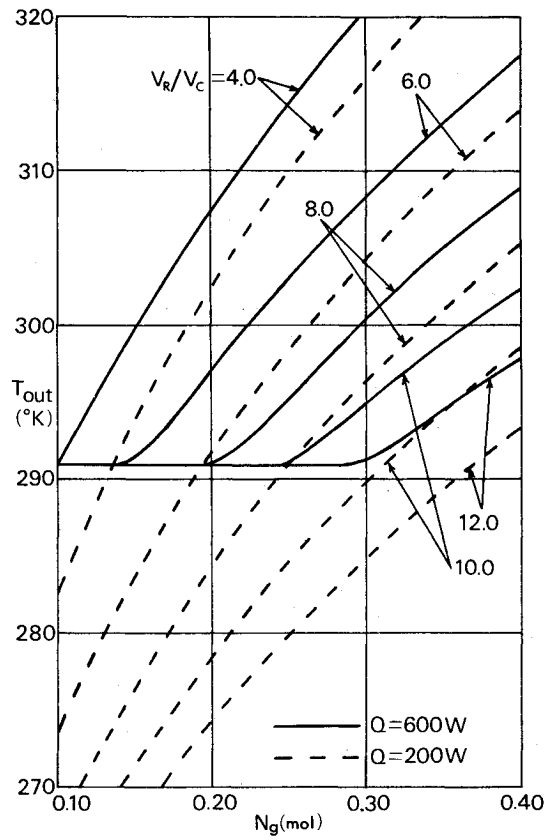


Fig. 5 Effect of reservoir volume on liquid outlet temperature (type 3).

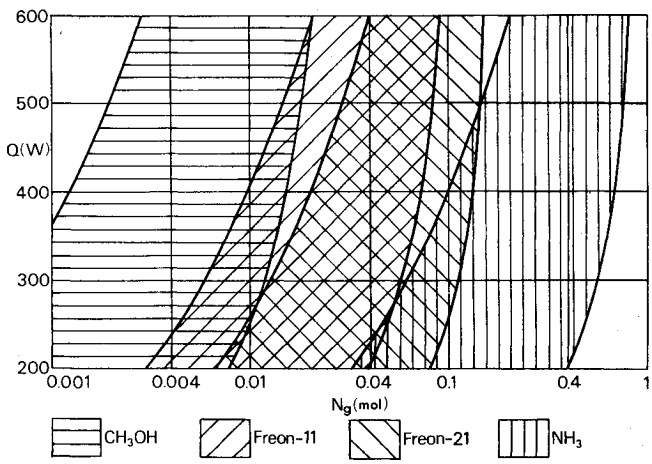


Fig. 6 Relation between nature of working fluids and nitrogen gas loading (type 3).

291.1 or 292.7 K when $T_s = 216$ K, $T_R = 227$ K, and $Q = 198$ or 462 W. Similar results, $T_B = 285$ or 291 K, are obtained in tests[4] performed under the same conditions.

Although both results are in good agreement, it should be pointed out that the tests[4] were done in a 1-atm ambient condition and that convection effects could not be entirely eliminated. Vacuum test data for the same radiator configuration are therefore required to infer a degree of convective transfer. The test results reported by Ward[5] are available for this purpose. For the type 3′ radiator, the tests[5] were conducted in a vacuum at three different sink temperatures of 239, 194, and 144 K. The averaged fin root temperatures[5] are as follows: 1) $T_B = 289$, 290, 291, and 295 K when $Q = 100$, 200, 300, and 381 W for the hot environment of 239 K; 2) $T_B = 280$, 284, and 290 K when $Q = 200$, 398, and 500 W for the cold environment of 194 K; and 3) $T_B = 282$ and

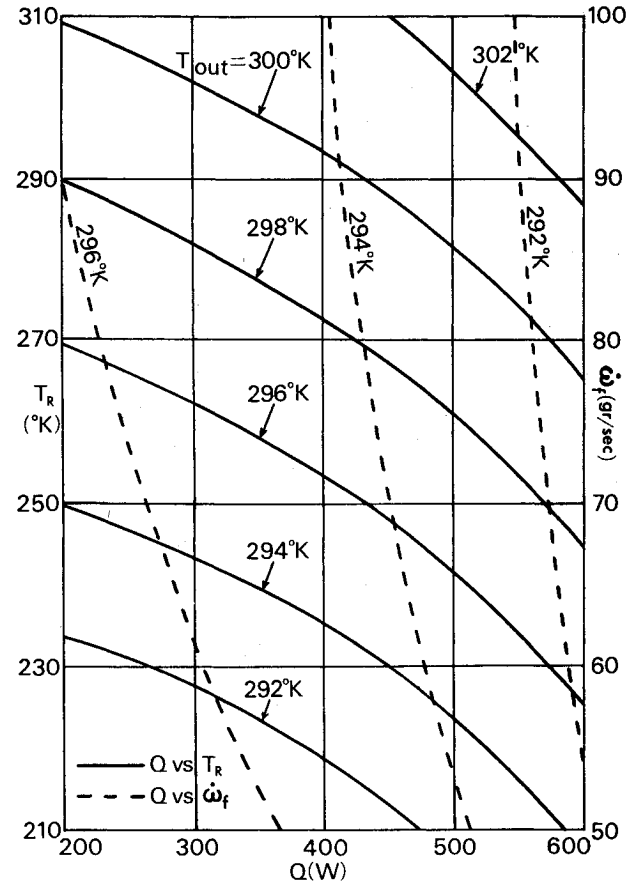


Fig. 7 Reservoir temperature or liquid flow rate vs heat load (type 3).

290 K when $Q = 500$ and 600 W for the colder environment of 144 K. The reservoir temperatures were then 239, 240, 241, and 254 K for the first series of testing; 200, 211, and 233 K for the second ones; and 199 and 234 K for the third ones. With such conditions as stated above, Eqs. (53), (54), and (49) yield the following results: 1) $T_B = 294.9$, 295.6, 296.4, and 298.3 K; 2) $T_B = 286.4$, 289.0, and 292.4 K; and 3) $T_B = 286.8$ and 291.9 K. Thus, the predicted temperatures are consistent not only with the test results[4] in the air but also with those[5] in the vacuum. This indicates that the convection effects are here small to a satisfactory degree.

Figure 4 displays the inlet and outlet liquid temperatures, $T_{in}$ and $T_{out}$, of type 2 and type 3 radiator systems operating at the sink temperature of 210 K; and, in addition, the midpoint temperature $T_4$ (0.5) of the fourth fin. The active condenser length $L_{a4}$ of the fourth heat pipe of the type 3 radiator is also plotted in the figure. From a two-dot chain line in Fig. 4, it is seen that the active condenser length $L_{a4}$ amounts to 1.83 m (full length) whenever the load $Q$ exceeds 560 W. In such a case, the fourth heat pipe no longer acts as a variable conductance heat pipe. It is then seen from Fig. 4 that a tighter control of the liquid temperature is obtained for the type 3 radiator system over that of type 2. The type 3 radiator system basically meets the performance requirement that the liquid outlet temperature should be maintained between 294 and 305 K over a load range of 200 to 600 W.

Parametric studies have been made to present technical knowledge available to design or operation of variable conductance heat pipe radiators (type 3). The results of prime importance are given in Figs. 5-7, to which the following data are common: $\lambda = 2.05$ W/cm·K, $h = 0.813$ mm, $\epsilon_0 = 0.90$, $\epsilon = 0.0$, $L = 1.83$ m, $L_e = 30.5$ cm, $W = 10.2$ cm, $N = 6$, $C_p = 1.05$ J/g·K, $\bar{\lambda}_e = 0.666$ W/cm·K, $\bar{\lambda}_c = 0.924$ W/cm·K, $V_c = 70.1$ cm$^3$, and $T_s = 210$ K. Unless otherwise provided, ammonia is chosen as working fluid and the following data are employed: $V_R = 547$ cm$^3$, $N_g = 0.25$ mole, $T_R = 228$ K, and $\dot{\omega}_f = 63.0$ g/s.

**Table 1 Inlet and outlet liquid temperatures of conical radiator (type 4)**

| | | | | $Q=400$ kW | | $Q=600$ kW | |
|---|---|---|---|---|---|---|---|
| $h$,mm | $L$,m | N | m, kg | $T_{in}$, K | $T_{out}$, K | $T_{in}$, K | $T_{out}$, K |
| | | 60 | 778 | 677.1 | 597.1 | 893.4 | 773.5 |
| | 7.0 | 70 | 803 | 608.0 | 528.1 | 763.4 | 643.5 |
| 1.5 | | 80 | 828 | 570.5 | 490.6 | 695.2 | 575.3 |
| | | 60 | 940 | 596.2 | 516.3 | 761.5 | 641.6 |
| | 9.0 | 70 | 970 | 548.8 | 468.8 | 673.7 | 553.8 |
| | | 80 | 1000 | 522.4 | 442.5 | 626.9 | 507.0 |
| | | 60 | 800 | 720.7 | 640.8 | 945.1 | 825.2 |
| | 5.0 | 70 | 820 | 649.5 | 569.6 | 812.0 | 692.1 |
| | | 80 | 840 | 610.8 | 530.9 | 741.9 | 622.0 |
| | | 60 | 988 | 611.8 | 531.8 | 770.5 | 650.6 |
| 2.0 | 7.0 | 70 | 1013 | 568.3 | 488.3 | 691.2 | 571.3 |
| | | 80 | 1037 | 543.9 | 464.0 | 648.4 | 528.5 |
| | | 60 | 1194 | 551.4 | 471.5 | 678.5 | 558.6 |
| | 9.0 | 70 | 1224 | 520.9 | 440.9 | 624.1 | 504.2 |
| | | 80 | 1253 | 503.2 | 423.2 | 594.0 | 474.1 |
| | | 60 | 970 | 665.8 | 585.9 | 842.2 | 722.3 |
| | 5.0 | 70 | 990 | 616.5 | 536.6 | 751.7 | 631.8 |
| | | 80 | 1010 | 588.6 | 508.6 | 702.8 | 582.9 |
| | | 60 | 1198 | 578.6 | 498.6 | 709.4 | 589.5 |
| 2.5 | 7.0 | 70 | 1222 | 547.4 | 467.5 | 654.6 | 534.7 |
| | | 80 | 1247 | 529.5 | 449.6 | 623.9 | 504.1 |
| | | 60 | 1447 | 528.1 | 448.2 | 636.9 | 517.0 |
| | 9.0 | 70 | 1477 | 505.9 | 425.9 | 598.3 | 478.4 |
| | | 80 | 1507 | 492.6 | 412.7 | 576.3 | 456.4 |
| | | 60 | 1139 | 633.8 | 553.9 | 783.3 | 663.5 |
| | 5.0 | 70 | 1159 | 596.5 | 516.5 | 716.4 | 596.5 |
| | | 80 | 1180 | 574.8 | 494.9 | 679.5 | 559.6 |
| 3.0 | | 60 | 1408 | 558.5 | 478.6 | 673.9 | 554.0 |
| | 7.0 | 70 | 1433 | 534.6 | 454.7 | 632.5 | 512.6 |
| | | 80 | 1457 | 520.4 | 440.4 | 608.7 | 488.8 |

In Fig. 5, the quantity of nitrogen gas, $N_g$, is plotted as abscissa against the Freon-21 outlet temperature $T_{out}$ as ordinate. The reservoir-to-condenser volume ratio, $V_R/V_c$, is taken as a parameter in Fig. 5. This figure serves as a basis of determining the optimal reservoir volume and the required gas quantity. In the case where the liquid outlet temperature is required to be maintained between 294 and 305 K, the volume ratio $V_R/V_c$ of 8.0 is desirable and the reservoir should be filled to the extent of 0.25 to 0.35 mole with gaseous nitrogen. A remarkable feature in Fig. 5 is that the liquid outlet temperature never falls below 291 K in any case where the heat load is 600 W. Such phenomena are due to the heat load exceeding the control limit, resulting from the fact that all the pipes then work as fixed- rather than variable-conductance heat pipes.

In general, too little quantity of control gas results in nearly fixed conductance. Excessive gas loading is also undesirable because of arresting the growth of active condenser length. Two limits are thus laid down as allowable gas quantities, producing such regions as the hatched portions in Fig. 6. This figure, in which the abscissa is expressed in logarithmic scale, can be used to find the gas quantities to be loaded in accordance with four sorts of working fluids widely used in heat pipe technology. For a load range of 200 to 600 W, the preferable amount of gaseous nitrogen is estimated at 0.003 to 0.008 mole for methyl alcohol, 0.02 to 0.04 mole for Freon-11, 0.04 to 0.08 mole for Freon-21, and 0.2 to 0.4 mole for ammonia.

Figure 7 displays liquid temperature control characteristics of a type 3 radiator system. The heat load $Q$ is here plotted as abscissa against the reservoir temperature $T_R$ as ordinate when $\dot{\omega}_f = 63.0$ g/s, and also against the liquid flow rate $\dot{\omega}_f$ as ordinate when $T_R = 228$ K. From two groups of curves in the figure, one can find the temperature $T_R$ or the flow rate $\dot{\omega}_f$

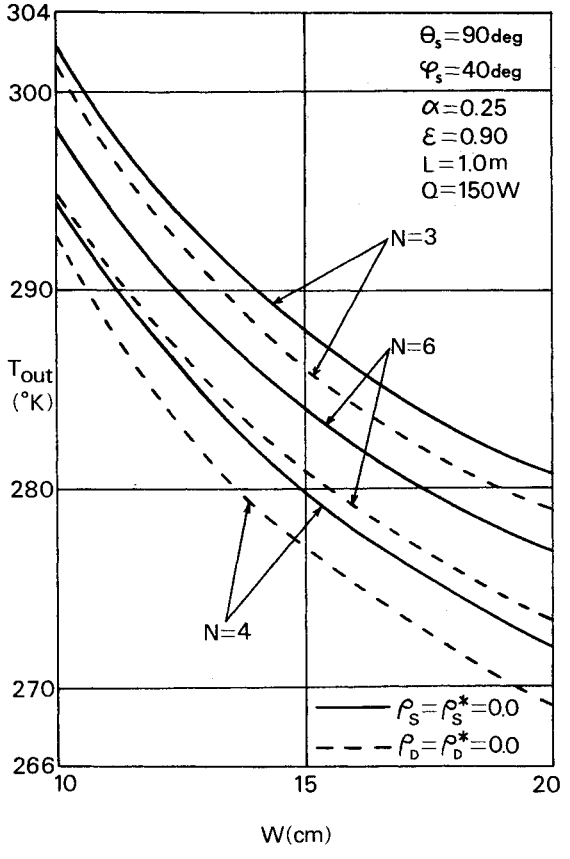


**Fig. 8 Effect of surface reflectances and number of fins on liquid outlet temperature (type 5).**

which should be controlled in response to the specified load $Q$ and the required outlet temperature $T_{out}$.

Now one considers a type 4 radiator configured as $r_1 = 2.06$ m and $r_2 = 6.60$ m and exposed to the solar radiation of 0.14 W/cm$^2$. The fins are made of beryllium, specified as 1.85 g/cm$^3$ in density, 2.05 W/cm·K in heat conductivity, and 0.25/0.90 in surface properties $\alpha/\epsilon$. The tubes are 4.38 cm in wetted perimeter and 1.36 W/cm$^2$·K in coefficient of heat transfer between liquid bulk and tube wall. The cooling liquid is Nak-78 of 0.878 J/g·K in specific heat at constant pressure, and is pumped at the mass flow rate of 5.7 kg/s. The inlet and outlet liquid temperatures, computed from Eqs. (65) and (66), are listed in Table 1 for a typical sun direction defined as defined as $\theta_s = \varphi_s = 90$ deg. For a space flight power system, the radiator is usually optimized to be lighter in weight and smaller in liquid temperature variation. If the design requirements are such that $h \geq 2.0$ mm for meteoroid protection, $m \leq 1200$ kg for mission attainability, and $440 \leq T_{out} \leq 500$ K over a load range of 400 to 600 kW, one then finds from Table 1 that an optimal radiator is 2.0 mm in thickness, 9.0 m in length, and 70 in number of tubes.

Figure 8 is here presented to illustrate the effect of fin surface nondiffusiveness on thermal control characteristics of a type 5 radiator. The data used for Fig. 8 are as follows: $\lambda = 2.05$ W/cm·K, $h = 1.0$ mm, $\alpha = 0.25$, $\epsilon = 0.90$, $L = 1.0$ m, $C_p = 1.05$ J/g·K, $\dot{\omega}_f = 63.0$ g/s, $h_f = 1.36$ W/cm$^2$·K, $p_w = 4.38$ cm, $I_s = 0.14$ W/cm$^2$, $\theta_s = 90$ deg, $\varphi_s = 40$ deg, and $Q = 150$ W. In Fig. 8, the liquid outlet temperature $T_{out}$ is plotted against the fin width $W$, and the number of fins, $N$, is taken as a design parameter. The curves represent the results for purely diffuse or purely specular surfaces, that is, for $\rho_S = \rho_S^* = 0.0$ or $\rho_D = \rho_D^* = 0.0$. As expected, the liquid outlet temperature is considerably influenced by both the surface reflectances and the number of fins.

## Concluding Remarks

Application of variational techniques has resulted in analytical expressions of fin surface temperature distributions of space radiators with pumped liquid circulation. These expressions have yielded a simple algorithm which permits accurate estimation of the inlet and outlet liquid temperatures. Based on this algorithm, a computer program has been developed for performance calculations of five types of radiators with or without heat pipes. The program can be used to determine the number of tubes or heat pipes needed and to optimize mass and dimensions of the radiator panel or cone. The validity of the program has been demonstrated by good agreement between numerical and experimental results for typical radiator configurations. Numerical computations have provided several charts which are useful in the design optimization of a variable conductance heat pipe radiator system.

## Appendix

Two sets of orthogonal coordinate systems are used for the analysis on radiative heat transfer in a V-groove cavity shown in the lower diagram of Fig. 3. The tube to which longitudinal fins are attached is chosen as the $X_3$ axis and as the $Z$ axis. The first fin plane contains the $X_1$ axis, from which the solar azimuth angle $\varphi_s$ is measured in the counterclockwise rotation. The $x$ axis is taken so as to be contained in the $n$th fin plane ($n = 1,2,\ldots,N$) and, therefore, intersects with the $X_1$ axis at an angle of $2\phi(n-1)$ where $\phi$ is defined as Eq. (56). The $n$th cavity consists of the outside surface of the $n$th fin and the inside surface of the $n+1$th fin, that is, surfaces 1 and 2.

The view factors between them are expressed as:

$$F_{12} = 1 - \sin\phi \qquad 0 < \phi < \pi/2 \tag{A1}$$

$$F_{1(2)1} = 1 - \sin 2\phi \qquad \text{if } 0 < \phi < \pi/4 \tag{A2a}$$

$$= 0 \qquad \text{if } \pi/4 \leq \phi < \pi/2 \tag{A2b}$$

$$F_{1(2,1)2} = 1 - \sin 3\phi \qquad \text{if } 0 < \phi < \pi/6 \tag{A3a}$$

$$= 0 \qquad \text{if } \pi/6 \leq \phi < \pi/2 \tag{A3b}$$

$$F_{1(2,1,2)1} = 1 - \sin 4\phi \qquad \text{if } 0 < \phi < \pi/8 \tag{A4a}$$

$$= 0 \qquad \text{if } \pi/8 \leq \phi < \pi/2 \tag{A4b}$$

$$F_{1(2,1,2,1)2} = 1 - \sin 5\phi \qquad \text{if } 0 < \phi < \pi/10 \tag{A5a}$$

$$= 0 \qquad \text{if } \pi/10 \leq \phi < \pi/2 \tag{A5b}$$

Equations (A2-A5) represent the generalized view factors. For better understanding of such factors, one takes the factor $F_{1(2,1,2,1)2}$ as an example. If surfaces 1 and 2 are perfect reflectors, this factor shows the proportion of radiation from surface 1 which arrives at surface 2 after four specular reflections.

The so-called semigray model can be employed to account for optical properties of fin surfaces. Thus they are specified by both the infrared emittance $\epsilon$ and the solar absorptance $\alpha$. The surface reflectances, $\rho$ and $\rho^*$, are then divided into diffuse and specular components dependent on the relations $\epsilon + \rho_S + \rho_D = 1$ and $\alpha + \rho_S^* + \rho_D^* = 1$. The asterisk is appended to indicate the solar wavelength region. The exchange factors are now expressible in the following series of specular components, $\rho_S$ and $\rho_S^*$, of the reflectances:

$$E_{12} = F_{12} + \rho_S^2 F_{1(2,1)2} + \rho_S^4 F_{1(2,1,2,1)2} + \cdots \tag{A6a}$$

$$E_{11} = \rho_S F_{1(2)1} + \rho_S^3 F_{1(2,1,2)1} + \cdots \tag{A6b}$$

$$E_{12}^* = F_{12} + \rho_S^{*2} F_{1(2,1)2} + \rho_S^{*4} F_{1(2,1,2,1)2} + \cdots \tag{A6c}$$

$$E_{11}^* = \rho_S^* F_{1(2)1} + \rho_S^{*3} F_{1(2,1,2)1} + \cdots \tag{A6d}$$

Since there is no difference between surfaces 1 and 2, the following relations hold:

$$E_{21} = E_{12} \qquad E_{22} = E_{11} \tag{A7a}$$

$$E_{21}^* = E_{12}^* \qquad E_{22}^* = E_{11}^* \tag{A7b}$$

Such reciprocity rules as Eqs. (A7) hold also for the absorption factors:

$$B_{21} = B_{12} \qquad B_{22} = B_{11} \tag{A8a}$$

$$B_{21}^* = B_{12}^* \qquad B_{22}^* = B_{11}^* \tag{A8b}$$

The factor $B_{ij}$ shows the proportion of radiation from surface $i$ which is eventually absorbed at surface $j$ after all possible intervening reflections. This results in the following expressions:

$$B_{11} = \epsilon E_{11} + \rho_D E_{11} B_{11} + \rho_D E_{12} B_{21} \tag{A9a}$$

$$B_{12} = \epsilon E_{12} + \rho_D E_{11} B_{12} + \rho_D E_{12} B_{22} \tag{A9b}$$

Because of Eq. (A8a), Eqs. (A9) reduce to simultaneous linear equations. Hence the solutions are readily obtained:

$$B_{11} = \epsilon\{(1 - \rho_D E_{11}) E_{11} + \rho_D E_{12}^2\} / \{(1 - \rho_D E_{11})^2 - (\rho_D E_{12})^2\} \tag{A10a}$$

$$B_{12} = \epsilon E_{12} / \{(1 - \rho_D E_{11})^2 - (\rho_D E_{12})^2\} \tag{A10b}$$

In the solar wavelength region, one finds the expressions similar to Eqs. (A10):

$$B^*_{I1}=\alpha\{(1-\rho^*_D E^*_{I1})E^*_{I1}+\rho^*_D E^{*2}_{I2}\}/\{(1-\rho^*_D E^*_{I1})^2 - (\rho^*_D E^*_{I2})^2\} \quad \text{(A11a)}$$

$$B^*_{I2}=\alpha E^*_{I2}/\{(1-\rho^*_D E^*_{I1})^2-(\rho^*_D E^*_{I2})^2\} \quad \text{(A11b)}$$

In analyzing the solar field in a V-groove cavity, it should be noted that there exist two different kinds of radiant flux originating from the incident sun beam. One of them consists of collimated flux, resulting from direct impingement or intervening specular reflections. The other is composed of randomly distributed flux due to diffuse reflections characterized by Eqs. (A8b) and (A11). Their contributions to the solar irradiance on surface $i$ ($i=1,2$) of the $n$th cavity are expressed in the coefficients $G_{ni}$ and $H_{ni}$, respectively. In the solar flux, $\Phi_n$, entering the $n$th cavity, the portion diffusely reflected from surface $i$ amounts to $\rho^*_D\Phi_n H_{ni}$, and $B^*_{il}$ of this quantity is eventually absorbed in the outside surface of the $n$th fin. Then only a part estimated at $\alpha\Phi_n G_{nl}$ is absorbed there without experiencing any diffuse reflections. The solar flux $\Phi_{\overline{n-1}}$ in the $n-1$th cavity behaves also in the same manner as $\Phi_n$. Thus one finds the solar energy, $q_n$, absorbed on the inside or outside surfaces of the $n$th fin:

$$q_n=\Phi_n(\alpha G_{n1}+\rho^*_D H_{n1}B^*_{I1}+\rho^*_D H_{n2}B^*_{I2}) + \Phi_{\overline{n-1}}(\alpha G_{\overline{n-1}2}+\rho^*_D H_{\overline{n-1}1}B^*_{I2}+\rho^*_D H_{\overline{n-1}2}B^*_{I1}) \quad \text{(A12)}$$

where $\Phi_n$ is expressed as:

$$\Phi_n=2I_s\sin\theta_s\sin\phi H_{sn}\eta(H_{sn}) \quad \text{(A13)}$$

The factor $H_{sn}$ is here defined as:

$$H_{sn}=\cos\{\varphi_s-\phi(2n-1)\} \quad \text{(A14)}$$

The coefficients $G_{ni}$ and $H_{ni}$ are obtainable provided that the specular reflection history is known for the incident sun beam. For this reason, the solar flux entering the cavity opening named surface 3 is divided into $M$ subflux ($M\gg 1$). The vector $\boldsymbol{r}_{nmj}$ is then introduced to specify the surface on which the $j$th specular reflection of the $m$th subflux ($m=1,2,\ldots,M$) takes place in the $n$th cavity. This vector is, therefore, equal to $\boldsymbol{e}_1$, $\boldsymbol{e}_2$, or $\boldsymbol{e}_3$ which identify surfaces 1, 2, or 3:

$$\boldsymbol{e}_1=\begin{pmatrix}1\\0\end{pmatrix},\quad \boldsymbol{e}_2=\begin{pmatrix}0\\1\end{pmatrix},\quad \boldsymbol{e}_3=\begin{pmatrix}0\\0\end{pmatrix} \quad \text{(A15)}$$

If the $m$th subflux eventually exits the cavity after $j$ specular reflections, then $\boldsymbol{r}_{nmj}=\boldsymbol{e}_3$. Since the expression $\rho^{*j-1}_S\boldsymbol{r}_{nmj}$ indicates the place and the rate of occurrence of the $j$th specular reflection, the specular reflection history of the $m$th subflux is generally expressed in terms of the vector $\boldsymbol{R}_{nm}$ defined as:

$$\boldsymbol{R}_{nm}=\boldsymbol{r}_{nm1}+\rho^*_S\boldsymbol{r}_{nm2}+\rho^{*2}_S\boldsymbol{r}_{nm3}+\cdots \quad \text{(A16)}$$

The coefficient $H_{ni}$ is now computed from Eq. (A16) in the following fashion:

$$H_{ni}=\lim_{M\to\infty}\sum_{m=1}^{M}\boldsymbol{R}_{nm}\boldsymbol{e}_i/M \quad \text{(A17)}$$

With a view to determining the coefficient $G_{ni}$, the vector $\boldsymbol{R}_{nm}$ is generalized so as to contain angular information on specular reflections. This leads to the vector $\boldsymbol{J}_{nm}$ defined as:

$$\boldsymbol{J}_{nm}=|\boldsymbol{D}_{nm0}\boldsymbol{n}_{nm1}|\boldsymbol{r}_{nm1}+\rho^*_S|\boldsymbol{D}_{nm1}\boldsymbol{n}_{nm2}|\boldsymbol{r}_{nm2} + \rho^{*2}_S|\boldsymbol{D}_{nm2}\boldsymbol{n}_{nm3}|\boldsymbol{r}_{nm3}+\cdots \quad \text{(A18)}$$

The vector $\boldsymbol{n}_{nmj}$ shows a unit vector normal to the surface on which the $j$th specular reflection occurs. This vector is, therefore, given by either $\boldsymbol{N}_1$, $\boldsymbol{N}_2$, or $\boldsymbol{N}_3$ which are unit in size and perpendicular to surfaces 1, 2, or 3:

$$\boldsymbol{N}_1=\begin{pmatrix}0\\1\end{pmatrix},\quad \boldsymbol{N}_2=\begin{pmatrix}\sin 2\phi\\-\cos 2\phi\end{pmatrix},\quad \boldsymbol{N}_3=\begin{pmatrix}\cos\phi\\\sin\phi\end{pmatrix} \quad \text{(A19)}$$

The vector $\boldsymbol{D}_{nmj}$ ($j=1,2,\ldots$), associated with $\boldsymbol{n}_{nmj}$, expresses the direction toward which the $m$th subflux turns after $j$ specular reflections, but the vector $\boldsymbol{D}_{nm0}$ simply expresses the direction of the solar flux incident on the $n$th cavity. Hence they are written as:

$$\boldsymbol{D}_{nmj}=\begin{pmatrix}l_{nmj}\\m_{nmj}\end{pmatrix},\quad \boldsymbol{D}_{nm0}=\begin{pmatrix}\sin\theta_s\cos\{\varphi_s-2\phi(n-1)\}\\\sin\theta_s\sin\{\varphi_s-2\phi(n-1)\}\end{pmatrix} \quad \text{(A20)}$$

One then finds the expression similar to Eq. (A17):

$$G_{ni}=\lim_{M\to\infty}\sum_{m=1}^{M}\boldsymbol{J}_{nm}\boldsymbol{e}_i/M \quad \text{(A21)}$$

Equations (A17) and (A21) can be numerically evaluated if one has all the details of $\boldsymbol{R}_{nm}$ and $\boldsymbol{J}_{nm}$. An attempt, based on three-dimensional analytical geometry, is therefore made to present equations which make possible to determine $\boldsymbol{r}_{nmj}$, $\boldsymbol{n}_{nmj}$, and $\boldsymbol{D}_{nmj}$. Such equations are derived from Fresnel's law of reflection, and finally reduce to a series of expressions suitable for application of iterative technique. This results in a program for the iteration starting with

$$\boldsymbol{r}_{nm0}=\boldsymbol{e}_3 \quad \text{(A22a)}$$

$$l_{nm0}=\sin\theta_s\cos\{\varphi_s-2\phi(n-1)\},\quad m_{nm0}=\sin\theta_s\sin\{\varphi_s-2\phi(n-1)\} \quad \text{(A22b)}$$

$$p_{nm}=\sin\theta_s[\sin(\varphi_s-2n\phi)+2\sin\phi\times\cos\{\varphi_s-\phi(2n-1)\}(m-\tfrac{1}{2})/M] \quad \text{(A22c)}$$

The parameter $p_{nm}$ is here introduced to specify the distance from the origin. The iteration is carried out in the following manner. First, if the conditions:

$$0<p_{nm}/m_{nmj}<1 \quad \text{and} \quad \boldsymbol{r}_{nmj}\boldsymbol{e}_1=0 \quad \text{(A23)}$$

hold, then one has:

$$\boldsymbol{r}_{nmj+1}=\boldsymbol{e}_1 \qquad \boldsymbol{n}_{nmj+1}=\boldsymbol{N}_1 \quad \text{(A24a)}$$

$$l_{nmj+1}=-l_{nmj} \qquad m_{nmj+1}=m_{nmj} \quad \text{(A24b)}$$

Second, if the conditions:

$$0<p_{nm}/(m_{nmj}\cos 2\phi-l_{nmj}\sin 2\phi)<1 \quad \text{and} \quad \boldsymbol{r}_{nmj}\boldsymbol{e}_2=0 \quad \text{(A25)}$$

hold, then one has:

$$\boldsymbol{r}_{nmj+1}=\boldsymbol{e}_2 \qquad \boldsymbol{n}_{nmj+1}=\boldsymbol{N}_2 \quad \text{(A26a)}$$

$$l_{nmj+1}=-l_{nmj}\cos 4\phi-m_{nmj}\sin 4\phi$$

$$m_{nmj+1}=m_{nmj}\cos 4\phi-l_{nmj}\sin 4\phi \quad \text{(A26b)}$$

If neither of the conditions (A23) and (A25) is satisfied, the iteration comes to an end. The results are then accompanied by:

$$r_{nmj+1} = e_3 \tag{A27}$$

## References


[1] Russell, L.D. and Chapman, A.J., "Analytical Solution of the 'Known-Heat-Load' Space Radiator Problem," *Journal of Spacecraft and Rockets,* Vol. 4, March 1967, pp. 311-315.

[2] Russell, L.D. and Chapman, A.J., "Analytical Solution for Transient Flow of Energy in a One-Dimensional Radiating Fin," *AIAA Journal,* Vol. 6, Jan. 1968, pp. 90-93.

[3] Roukis, J., Rogovin, J., and Swerdling, B., "Heat Pipe Applications to Space Vehicles," AIAA Paper 71-410, April 1971.

[4] Edelstein, F., "Deployable Heat Pipe Radiator," NASA/MSFC, Contract NAS 8-29905, DHPR-75-13, April 1975.

[5] Ward, T.L., "Space Tug Thermal Control Follow-on," NASA/MSFC, Contract NAS 8-30746, MCR-75-270, Oct. 1975.

[6] Alario, J. and Canaras, T., "Modular Heat Pipe Radiator," ASME Paper 77-ENAs-39, July 1977.

[7] Alario, J. and Haslett, R., "Modular Heat Pipe Radiators for Enhanced Shuttle Mission Capabilities," ASME Paper 79-ENAs-17, July 1979.

[8] Schlitt, R., "A Heat-Pipe Radiator for Shunt Electronics: Development and Test Results," *Proceedings of Thermal and Environmental Control Systems Symposium,* Nov. 1978, pp. 73-83.

[9] Tharpe, B.J. and Arker, A.J., "Nuclear Electric Power for Manned Space Stations," *Space Power Systems Engineering,* Academic Press, New York, 1966, pp. 51-113.

[10] Keil, H., "Optimization of a Central Fin Space Radiator," *Journal of Spacecraft and Rockets,* Vol. 5, April 1968, pp. 463-465.

[11] Hering, R.G., "Radiative Heat Exchange and Equilibrium Surface Temperature in a Space Environment," *Journal of Spacecraft and Rockets,* Vol. 5, Jan. 1968, pp. 47-54.

[12] Schnurr, N.M., "Radiation from an Array of Longitudinal Fins of Triangular Profile," *AIAA Journal,* Vol. 13, May 1975, pp. 691-693.

[13] Marcus, B.D., "Theory and Design of Variable Conductance Heat Pipes," NASA CR-2018, April 1972.

[14] Chi, S.W., *Heat Pipe Theory and Practice: A Sourcebook,* Washington Hemisphere Publishing Co., 1976.

[15] Gregg, G.E. et al., *SAE Aerospace Applied Thermodynamic Manual,* Society of Automotive Engineers, 1969.

[16] Scollon, T.R. Jr. and Carpitella, M.J., "Long Life High Reliability Thermal Control Systems Study Data Handbook," NASA/MSFC, Contract NAS 8-26252, NASA CR-123734, Dec. 1971.

[17] Skrabek, E.A., "Heat Pipe Design Handbook," NASA/MSC, Contract NAS 9-11927, DTM-72-3, Aug. 1972.